Smart Structures and Systems, *Vol. 32, No. 6 (2023) 393-402*
https://doi.org/10.12989/sss.2023.32.6.393

Multi-spectral adaptive vibration suppression of two-path active mounting systems with multi-NLMS algorithms

Yang Qiu [1a], Dongwoo Hong [2a] and Byeongil Kim*[1]

[1] *School of Mechanical Engineering, Yeungnam University, Gyeongsan 38541, South Korea*
[2] *Daegu Mechatronics & Materials Institute, Daegu 42714, South Korea*

(*Received July 17, 2022, Revised January 9, 2023, Accepted November 23, 2023*)

Abstract. Recently, hybrid and electric vehicles have been actively developed to replace internal combustion engine (ICE) vehicles. However, their vibrations and noise with complex spectra cause discomfort to drivers. To reduce the vibrations transmitted through primary excitation sources such as powertrains, structural changes have been introduced. However, the interference among different parts is a limitation. Thus, active mounting systems based on smart materials have been actively investigated to overcome these limitations. This study focuses on diminishing the source movement when a structure with two active mounting systems is excited to a single sinusoidal and a multi-frequency signal, which were investigated for source movement reduction. The overall structure was modeled based on the lumped parameter method. Active vibration control was implemented based on the modeled structure, and a multi-normalization least mean square (NLMS) algorithm was used to obtain the control input for the active mounting system. Furthermore, the performance of the NLMS algorithm was compared with that of the quantification method to demonstrate the performance of active vibration control. The results demonstrate that the vibration attenuation performance of the source component was improved.

Keywords: active engine mounting; beam structure; mathematical quantification method; multi-NLMS algorithm; piezoelectric actuator

1. Introduction

Hybrid and electric vehicles are being actively developed to replace conventional ICE vehicles. In addition, downsizing and high-efficiency powertrains are required to produce lightweight high-performance vehicles. However, they cause noise, vibration, and harshness (NVH) in vehicles. The most common cause of these problems is the midfrequency vibrations that occur in electric vehicles. The excitation force of the engine causes secondary vibrations through other parts, such as the subframe, body, and powertrain, which cause discomfort to the driver. To overcome the NVH problem, structural modifications are typically performed; however, this is limited by the interference of parts with each other. To overcome this problem, active vibration control based on smart materials is applied in engine mounts. Several studies have developed high-performance active mounting systems.

Lead zirconate titanate (PZT) actuators are widely used in mounting systems to control vibrations (Xiong and Shi 2012, Vijayakumar *et al*. 2014, Choi and Hong 2007, Choi *et al*. 2008, Sohn *et al*. 2010). Garcia-Bonito *et al*. (1998) proposed a hydraulic actuator that applies a PZT ring and showed that a high force and relatively high displacements can be produced. Lu *et al*. (2020) recommends a piezoelectric inertial vertical isolation system (PIVIS) to improve vertical vibration isolation performance. Jiang *et al*. (2018) constructed a structure–actuator interaction (SAI) according to magnetomechanical coupling, and their experiments revealed that the stiffness effect increased. Furthermore, to increase the control performance and stability, smart materials are combined with other elements such as rubber, fluid, and wire. Simonovic *et al*. (2016) presented a design and experimental verification of the active vibration control system of an aluminum plate, and the proposed control system exhibited a high level of effectiveness in active vibration damping. Shin *et al*. (2019) proposed an active hybrid mount using wire mesh material and an inertial mass-type actuator. Through experiments, the vibration reduction effect was validated. Han (2020) proposed an active hybrid mounting system comprising a piezoelectric actuator and rubber element to improve the integrated starter–generator (ISG) vibration characteristics at the initial start, and the ISG vibration characteristics were improved. Also, actuators and sensors are widely applied to smart composite structures. (Chee *et al*. 1999, Malgaca and Karagulle 2009). Vivek *et al*. (2011) presented an analytical procedure for actively controlling piezoelectric smart structures and the results are very helpful for analyzing beam and plate structures with actively controlling piezoelectric. ALamir (2015) according to Liapunov-Bellman principle and formulations from various plate theories for various boundary conditions, the feasibility of optimal control and design for composite laminates was

*Corresponding author, Ph.D., Professor,
E-mail: bikim@yu.ac.kr
[a] Ph.D.

ISSN: 1738-1584 (Print), 1738-1991 (Online)

confirmed.

In addition, several studies have developed active control algorithms, such as the H-infinity algorithm (Zhao and Wang 2019), multi-normalization least mean square (NLMS) algorithm (Hong and Kim 2019a, b), and fuzzy control (Lin and Jheng 2017). Hillis *et al*. (2005) proposed an error-driven minimal controller synthesis (Er-MCSI), which is applied to active engine mounts consisting of a passive mount and an internal electromagnetic actuator. Song and Zhao (2018) proposed the filtered-x generalized mixed norm (FXGMN) and a combination of the FXGMN algorithm to overcome the limitations of the adaptive filtering algorithm and showed that a better convergence speed and higher noise reduction can be achieved. Gao *et al*. (2020) suggested a FX-VSSA-LMS algorithm to realize real-time active vibration of the cantilever beam. The performance of vibration suppression was confirmed experimentally when the different load for cantilever beam. Niu *et al*. (2019) proposed an enhancement of the classical Fx-LMS algorithm to overcome the limitation of secondary path estimation. Their proposed method was confirmed to be effective for suppressing the vibration of time-varying systems. Naseri *et al*. (2020) proposed an active vibration control method comprising a robust active controller and disturbance observer for active engine mounts and showed that the transmitted vibration was significantly reduced. Jang *et al*. (2015) presented an active mass damper system with time delay control algorithm for a small three-story building structure model on a shaking table. Vibration control performance is well verified by conducting free vibration and forced vibration experiments. Lee *et al*. (2018) proposed an optimized weights-FxLMS (OW-FxLMS) to reduce the noise inside the cabin of a car and showed that the engine noise was significantly reduced. Kim *et al*. (2012a, b, 2013) proposed a model predictive sliding mode control algorithm to improve the performance of conventional LMS algorithms. The vibration reduction performance was validated experimentally, which showed that vibrations were attenuated for the piezoelectric strut structure and cantilever beam. Cao *et al*. (2021) advised a genetic algorithm (GA), which is applied to smart composite beam and constructed that GA can well control the vibration under certain conditions. Liette *et al*. (2014) implemented vibration control for the source-path-receiver structure consisting of two active paths. The active paths were combined with a piezoelectric actuator and a rubber grommet. To isolate the source motion, the active path input signal was quantified by considering the interaction between the source and active paths. Through simulations and experiments, vibration isolation was validated at the targeted source path.

However, this quantification method exhibited several limitations. When vibration control is implemented, the overall vibration ought to decrease. However, in the quantification method, only the targeted path was found to isolate the vibration. Thus, the other path did not contribute to vibration reduction. Additionally, an actual engine generates a complex signal consisting of three or four frequencies. However, the quantification method can only be applied to a single sinusoid; thus, it is difficult to apply in an actual engine mounting system.

Thus, the scope of this study is restricted to controlling the movement at the source component for a single sinusoid and multi-frequency signal in the midfrequency range. To diminish the source movement, a streamlined active structure consisting of two active paths was investigated, as shown in Fig. 1.

In Fig. 1, the source component represents the electric power train; the paths represent the active path consisting of the piezoelectric actuator and rubber grommet, and the receiver component represents the subframe. The specific objectives of this study are summarized as follows: 1) The NLMS algorithm was applied to the active engine mount system to validate the vibration reduction performance, and it was compared to the quantification method. 2) To confirm the vibration reduction effect at complex signals exhibiting multi-frequency, the multi-NLMS algorithm was applied to the active mounting system. The overall structure was modeled based on the lumped parameter model to investigate the vibration reduction effect in the midfrequency range. When the simulation is performed, the system is discrete, independent of frequency, and considers linear motion without nonlinear kinematic effects. In the active paths, only a piezoelectric actuator contributes to the mass, and the hysteresis effect of the piezoelectric actuator was neglected. Additionally, the rotational motion was small in the source and receiver parts, and the perturbation force was only applied in the source component. When the perturbation force was considered, a single sinusoid and multiple frequencies were applied to attenuate the vibration in the midfrequency range. Additionally, the translation motion was considered only in the vertical motion. Furthermore, the NLMS algorithm was applied to control the system through an active mounting system. Through simulation, the effect of mitigating the source movement was validated based on active mounting systems.

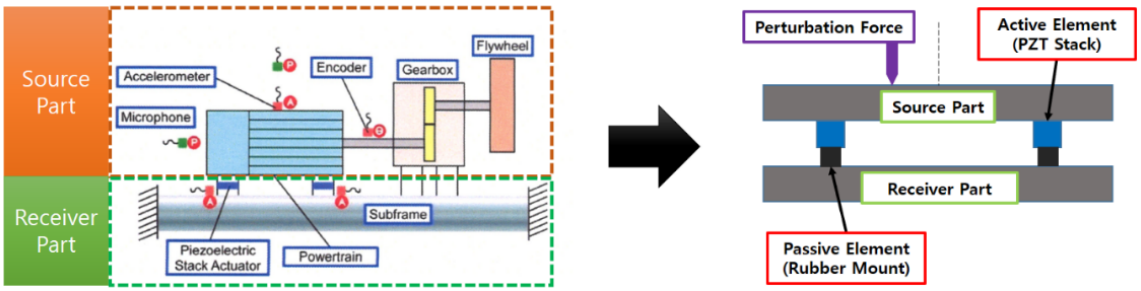

Fig. 1 Active element integration for mitigating source movement from perturbation force

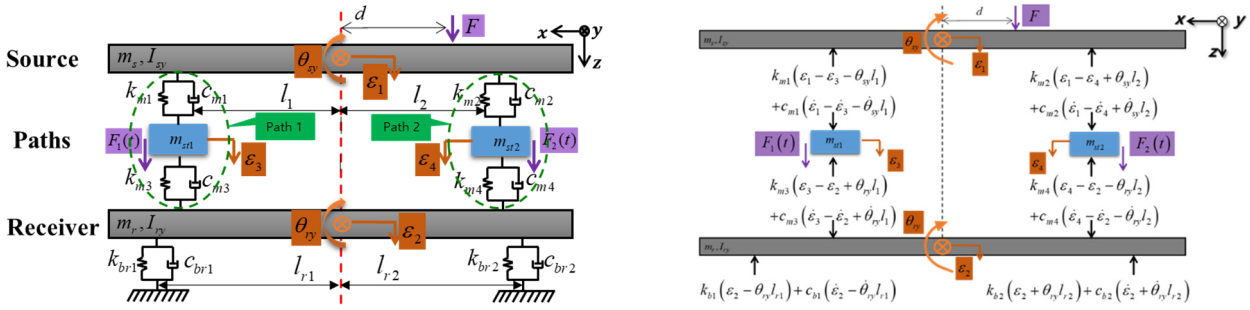

Fig. 2 Six-DOF lumped parameter model and free-body diagram

The remainder of this paper is organized as follows: Section 2 describes the system modeling, consisting of two active paths, and the quantification method for the active mounting system input. Section 3 compares the results between the quantification method and NLMS algorithm for a single sinusoid. Additionally, the simulation results for multiple frequencies are summarized for amplitude- and frequency-modulated signals. Finally, Section 4 presents the conclusions and discusses the scope for future studies.

2. Mounting system modeling

2.1 Lumped parameter model

The overall model consisting of the source-path-receiver was modeled based on the lumped parameter model, as shown in Fig. 1. In Fig. 1(a), the source component represents the electric and hybrid engine, the paths represent an active mounting system consisting of a piezoelectric stack actuator and a rubber grommet, and the receiver represents the subframe. A free-body diagram of the modeled structure is shown in Fig. 1(b). In this study, displacement and rotational motion were considered only in the z- and y-directions, respectively.

In Fig. 2, m_s and m_r represent the masses of the source and receiver, respectively. m_{st1} and m_{st2} are the masses of the piezoelectric stack actuator. Each mass was used as a realistic value through the measurement, and the mass of the rubber mount was ignored. I_{sy} and I_{ry} represent the moments of inertia in the y-direction, corresponding to the source and receiver, respectively. l_{r1} and l_{r2} are the lengths between the center of mass and Paths 1 and 2, respectively. d represents the length from the center of mass corresponding to the shaker. k_{mi} and k_{bti} represent the complex stiffness in each path corresponding to between the source and receiver, and between the receiver and ground, respectively. ε_i represents the displacement of the vertical motion in the z-direction. θ_{sy} and θ_{ry} represent the rotational displacements in the y-direction, corresponding to the source and receiver, respectively. F_i represents the actuator force in each path, and F represents the disturbance force. There are four translational motions for each mass in the z-direction and two rotational motions for the source and receiver in the y-direction. They can be expressed by forming an equation of motion according to Newton's 2nd law.

$$\boldsymbol{M}\ddot{\boldsymbol{q}}(t) + \boldsymbol{C}\dot{\boldsymbol{q}}(t) + \boldsymbol{K}\boldsymbol{q}(t) = \boldsymbol{F}(t) + \boldsymbol{W}(t) \tag{1}$$

$$\boldsymbol{M} = diag(\{m_s \quad m_r \quad m_{st1} \quad m_{st2} \quad I_{sy} \quad I_{ry}\}) \tag{2}$$

In Eqs. (1)-(5), M, q(t), W(t), and F(t) represent the mass, displacement, disturbance force, and control-force vectors, respectively. K and C represent the stiffness and damping matrices, respectively.

$$\boldsymbol{K} = \begin{bmatrix} k_{m1}+k_{m2} & 0 & -k_{m1} & -k_{m2} & k_{m2}l_2 - k_{m1}l_1 & 0 \\ 0 & k_{m3}+k_{m4}+k_{b1}+k_{b2} & -k_{m3} & -k_{m4} & 0 & k_{m4}l_2 - k_{m3}l_1 + k_{b2}l_{r2} - k_{b1}l_{r1} \\ -k_{m1} & -k_{m3} & k_{m1}+k_{m3} & 0 & k_{m1}l_1 & k_{m3}l_1 \\ -k_{m2} & -k_{m4} & 0 & k_{m2}+k_{m4} & -k_{m2}l_2 & -k_{m4}l_2 \\ k_{m2}l_2 - k_{m1}l_1 & 0 & k_{m1}l_1 & -k_{m2}l_2 & k_{m1}l_1^2 + k_{m2}l_2^2 & 0 \\ 0 & k_{m4}l_2 - k_{m3}l_1 + k_{b2}l_{r2} - k_{b1}l_{r1} & k_{m3}l_1 & -k_{m4}l_2 & 0 & k_{m3}l_1^2 + k_{m4}l_2^2 + k_{b1}l_{r1}^2 + k_{b2}l_{r2}^2 \end{bmatrix} \tag{3}$$

$$\boldsymbol{C} = \begin{bmatrix} c_{m1}+c_{m2} & 0 & -c_{m1} & -c_{m2} & c_{m2}l_2 - c_{m1}l_1 & 0 \\ 0 & c_{m3}+c_{m4}+c_{b1}+c_{b2} & -c_{m3} & -c_{m4} & 0 & c_{m4}l_2 - c_{m3}l_1 + c_{b2}l_{r2} - c_{b1}l_{r1} \\ -c_{m1} & -c_{m3} & c_{m1}+c_{m3} & 0 & c_{m1}l_1 & c_{m3}l_1 \\ -c_{m2} & -c_{m4} & 0 & c_{m2}+c_{m4} & -c_{m2}l_2 & -c_{m4}l_2 \\ c_{m2}l_2 - c_{m1}l_1 & 0 & c_{m1}l_1 & -c_{m2}l_2 & c_{m1}l_1^2 + c_{m2}l_2^2 & 0 \\ 0 & c_{m4}l_2 - c_{m3}l_1 + c_{b2}l_{r2} - c_{b1}l_{r1} & c_{m3}l_1 & -c_{m4}l_2 & 0 & c_{m3}l_1^2 + c_{m4}l_2^2 + c_{b1}l_{r1}^2 + c_{b2}l_{r2}^2 \end{bmatrix} \tag{4}$$

$$q(t) = \begin{Bmatrix} \varepsilon_1(t) \\ \varepsilon_2(t) \\ \varepsilon_3(t) \\ \varepsilon_4(t) \\ \theta_{sy}(t) \\ \theta_{ry}(t) \end{Bmatrix} W(t) = \begin{Bmatrix} F(t) \\ 0 \\ 0 \\ 0 \\ F(t)d_1 \\ 0 \end{Bmatrix} F(t) = \begin{Bmatrix} 0 \\ 0 \\ F_1(t) \\ F_2(t) \\ 0 \\ 0 \end{Bmatrix} \tag{5}$$

Table 1 Identified system parameters

Parameters	Values	Unit
$m_s = m_r$	1.395	K_g
$m_{st1} = m_{st2}$	0.075	K_g
$I_{sy} = I_{ry}$	18.675	gm^2
k_{m1}	$5.64(1 + i0.036)$	KN/mm
k_{m2}	$2.48(1 + i0.036)$	KN/mm
k_{m3}	$0.61(1 + i0.300)$	KN/mm
k_{m4}	$0.530(1 + i0.300)$	KN/mm
k_{brn}	$0.420(1 + i0.300)$	KN/mm
d	67	mm
l_1	67	mm
l_2	118	mm
$l_{r1} = l_{r2}$	189	mm

The equation of motion was derived from the center-of-mass coordinates. To confirm the effect of the vibration reduction in each path, the center-of-mass coordinates ought to be changed to each active mount coordinate, as shown in Fig. 3. In Fig. 3, points A, B, and O represent the positions of Actuators 1 and 2, and the center of gravity, respectively. To transform the coordinates, the internally dividing point was applied, which can be expressed as Eq. (6).

$$O = \frac{l_2}{l_1 + l_2} A + \frac{l_1}{l_1 + l_2} B \tag{6}$$

$$\Pi = \begin{bmatrix} \frac{l_2}{l_1+l_2} & \frac{l_1}{l_1+l_2} & 0 & 0 & 0 & 0 \\ 0 & 0 & 0 & 0 & \frac{l_2}{l_1+l_2} & \frac{l_1}{l_1+l_2} \\ 0 & 0 & 1 & 0 & 0 & 0 \\ 0 & 0 & 0 & 1 & 0 & 0 \\ \frac{-1}{l_1+l_2} & \frac{1}{l_1+l_2} & 0 & 0 & 0 & 0 \\ 0 & 0 & 0 & 0 & \frac{-1}{l_1+l_2} & \frac{1}{l_1+l_2} \end{bmatrix} \tag{7}$$

The transformed displacement is defined by Eq. (8): The equation of motion according to the transformed coordinate

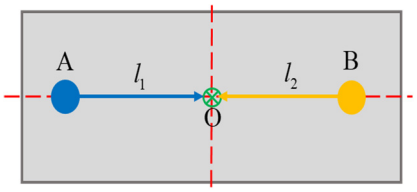

Fig. 3 Positional relationship between Actuators 1 and 2

is rewritten using Eq. (9). The vector of the amplitude displacement corresponding to each path is defined by Eq. (10). A schematic of the transformed coordinates is expressed in Fig. 4.

$$\boldsymbol{q(t)} = \prod \boldsymbol{q^*(t)} \tag{8}$$

$$M^*\ddot{q}^*(t) + C^*\dot{q}^*(t) + K^*q^*(t) = F(t) + W(t) \tag{9}$$

$$q^*(t) = \{\xi_{p1g1} \quad \xi_{p2g1} \quad \varepsilon_3 \quad \varepsilon_4 \quad \xi_{p1g2} \quad \xi_{p2g2}\}^T \tag{10}$$

2.2 Control force and phase derivation (quantification method)

The calculation of the control force and phase of the two active paths are required to confirm the vibration isolation effect. Therefore, the excitation force and control forces are defined as harmonic excitations, as shown in Eqs. (11)-(12).

$$F(t) = W_1 e^{i\omega t} \tag{11}$$

$$F_i^*(t) = F_i e^{i(\omega t + \phi_{sti})} \tag{12}$$

W_1 and F_i denote the amplitudes of the shaker and ith actuators, respectively. ϕ_{sti} stands for the phase of ith actuators. To simplify the notation, the displacement is rewritten as shown in Eq. (13).

$$\xi_i^*(t) = \xi_{pig1}^*(t) \tag{13}$$

In Eq. (13), $\xi_i^*(t)$ should be zero to isolate the source movement. As the system is linear, the source movement can be defined as shown in Eq. (14).

$$\xi_i^*(t) = (\Xi_{si,1}^* + \Xi_{si,st1}^* e^{i\phi_{st1}} + \Xi_{si,st2}^* e^{i\phi_{st2}}) e^{i\omega t} \tag{14}$$

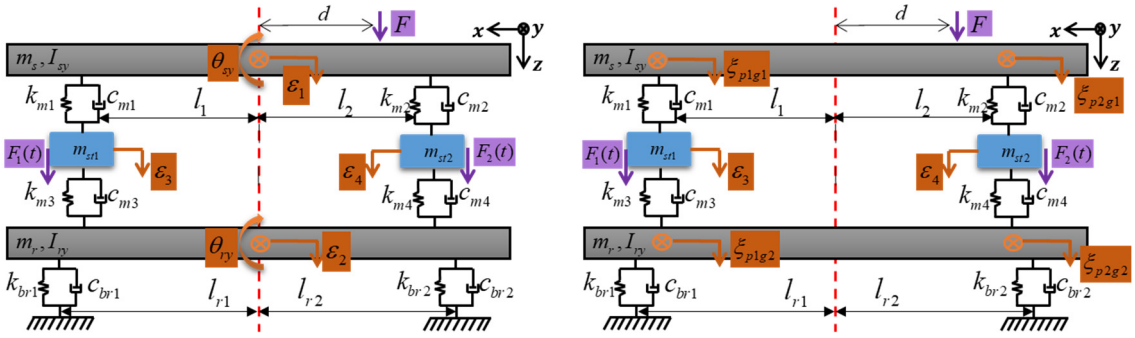

(a) Before coordinate change (b) New coordinate at attachments of active or passive mount

Fig. 4 Schematic representation

$$\begin{Bmatrix} F_1 \\ F_2 \end{Bmatrix} = \frac{F}{\left|H_{13}^{*'}\right|\left|H_{24}^{*'}\right| - \left|H_{14}^{*'}\right|\left|H_{23}^{*'}\right|} \begin{Bmatrix} \left|H_{14}^{*'}\right|\left|H_{21}^{*'}+\mathrm{dH}_{25}^{*'}\right| - \left|H_{24}^{*'}\right|\left|H_{11}^{*'}+\mathrm{dH}_{15}^{*'}\right| \\ \left|H_{23}^{*'}\right|\left|H_{11}^{*'}+\mathrm{dH}_{15}^{*'}\right| - \left|H_{13}^{*'}\right|\left|H_{21}^{*'}+\mathrm{dH}_{25}^{*'}\right| \end{Bmatrix} \tag{22}$$

In Eq. (14), $\Xi_{si,1}^{*}$, $\boldsymbol{\Xi}_{si,st1}^{*}$, and $\boldsymbol{\Xi}_{si,st2}^{*}$ represent the complex amplitudes owing to $w_1^*(t)$, Actuator 1, and Actuator 2. The dynamic stiffness matrix is defined as $\kappa^* = -\omega^2 M^* + i\omega C^* + K^*$, and the complex compliance matrix $H^{*'}$ can be obtained using Eq. (15).

$$\boldsymbol{H}^{*'} = \begin{bmatrix} H_{11}^{*'} & H_{12}^{*'} & H_{13}^{*'} & H_{14}^{*'} & H_{15}^{*'} & H_{16}^{*'} \\ H_{21}^{*'} & H_{22}^{*'} & H_{23}^{*'} & H_{24}^{*'} & H_{25}^{*'} & H_{26}^{*'} \\ H_{31}^{*'} & H_{32}^{*'} & H_{33}^{*'} & H_{34}^{*'} & H_{35}^{*'} & H_{36}^{*'} \\ H_{41}^{*'} & H_{42}^{*'} & H_{43}^{*'} & H_{44}^{*'} & H_{45}^{*'} & H_{46}^{*'} \\ H_{51}^{*'} & H_{52}^{*'} & H_{53}^{*'} & H_{54}^{*'} & H_{55}^{*'} & H_{56}^{*'} \\ H_{61}^{*'} & H_{62}^{*'} & H_{63}^{*'} & H_{64}^{*'} & H_{65}^{*'} & H_{66}^{*'} \end{bmatrix} \tag{15}$$

The magnitude and phase of the ith active path are defined by Eqs. (16)-(17) based on the compliance matrix, as follows

$$\Xi_{si,l}^{*} = \left(H_{il}^{*'} + H_{i5}^{*'} d\right) W_1, \quad \Xi_{si,stj}^{*} = H_{i3}^{*'} F_j \tag{16}$$

$$\beta_{\mathrm{si,1}} = \angle\left(H_{\mathrm{i1}}^{*'} + \mathrm{H}_{\mathrm{i5}}^{*'} d\right), \beta_{\mathrm{si,stj}} = \angle H_{\mathrm{i3}}^{*'} \tag{17}$$

In Eq. (17), $\angle$ represents the phase operator; $\beta_{si,1}$ denotes the phase generated by the disturbance force; and $\beta_{si,stj}$ denotes the phase generated by the jth actuator in the ith path. Eq. (14) is rewritten with respect to magnitude and phase based on Eqs. (16)-(17), as shown in Eq. (18).

$$\begin{aligned} \xi_i^*(t) = (&\left|\Xi_{\mathrm{si,1}}^{*}\right| e^{i\beta_{si,1}} + \left|\Xi_{\mathrm{si,st1}}^{*}\right| e^{i(\beta_{si,st1}+\phi_{st1})} \\ &+ \left|\Xi_{\mathrm{si,st2}}^{*}\right| e^{i(\beta_{si,st2}+\phi_{st2})}) e^{\mathrm{i\omega t}} \end{aligned} \tag{18}$$

Eq. (18) comprises five phase terms. Three phases were generated by the shaker and actuator, and two phases occurred only in the actuator. Owing to these issues, motion control is difficult to achieve. Thus, to achieve motion control, phase matching is implemented for the shaker. Through this assumption, an out-of-phase motion can be created. Therefore, the phase of ith path can be written as $\beta_{s1,1} = \beta_{s1,sti} + \phi_{sti}$ and thereafter can be summarized as Eq. (19).

$$\phi_{sti} = \beta_{s1,1} - \beta_{s1,sti} \tag{19}$$

The phase-matching Eq. (20) is obtained by substituting Eq. (19) into Eq. (18).

$$\xi_i^*(t) = (\left|\Xi_{si,1}^{*}\right| + \left|\Xi_{si,st1}^{*}\right| + \left|\Xi_{si,st2}^{*}\right|) e^{i(\omega t + \beta_{si,1})} \tag{20}$$

To isolate the vibration in the source component, the input force of the active mounting system was calculated, assuming that the magnitude term was zero. Therefore, the magnitude term in Eq. (20) can be defined by Eq. (21) as follows

$$\left|\Xi_{si,1}^{*}\right| + \left|\Xi_{si,st1}^{*}\right| + \left|\Xi_{si,st2}^{*}\right| = 0 \tag{21}$$

Finally, the actuator force is defined by Eq. (22).

3. Numerical validation

3.1 State-space model

To validate the vibration reduction effect on the source component, a simulation was performed using the state-space equation. The schematic and the equations of motion are shown in Fig. 5, and Eqs. (23)-(24), respectively.

$$\dot{x}(t) = Ax(t) + Bu(t) \tag{23}$$

$$y(t) = Cx(t) + Du(t) \tag{24}$$

In Eqs. (23)-(24), A, B, and C represent the system, input, and output state matrices, respectively, which are defined by Eqs. (25)-(26).

$$A = \begin{bmatrix} O_{6\times6} & I_{6\times6} \\ -\dfrac{K^*}{M^*} & -\dfrac{C^*}{M^*} \end{bmatrix} B = \begin{bmatrix} O_{6\times6} \\ \dfrac{1}{M^*} \end{bmatrix} \tag{25}$$

$$C = \begin{bmatrix} I_{2\times2} & O_{2\times2} & O_{2\times2} & O_{4\times6} \\ O_{2\times2} & O_{2\times2} & I_{2\times2} \end{bmatrix} D = [O_{4\times6}] \tag{26}$$

M^*, C^*, and K^* represent the mass, damping, and stiffness, respectively, after transformation. This study focuses on the vibration reduction performance of the source component through active mounting systems when a midfrequency perturbation signal is excited. Thus, the output $y(t)$ comprises four outputs, owing to the two source and receiver components for the active path, and it is defined by Eq. (27).

$$y(t) = \{a_{p1g1} \quad a_{p2g1} \quad a_{p1g2} \quad a_{p2g2}\}^T \tag{27}$$

Furthermore, the input signal is defined by Eqs. (28)-(30).

$$u(t) = 10\, sin(2\pi 460t) \tag{28}$$

$$u(t) = 4\, sin(2\pi 460t) \cdot [1 + cos(2\pi 160t)] \tag{29}$$

$$u(t) = 2\, sin(2\pi 460t + 2\, cos(2\pi 60t)) \tag{30}$$

The sinusoid in Eq. (28) is used to compare the vibration reduction performance between the quantification method and the NLMS algorithm. In addition, amplitude-

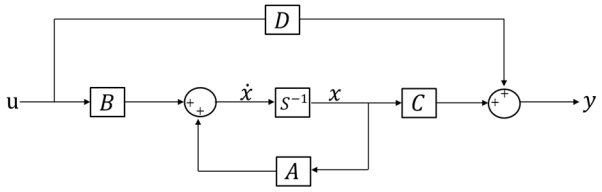

Fig. 5 State-space block diagram

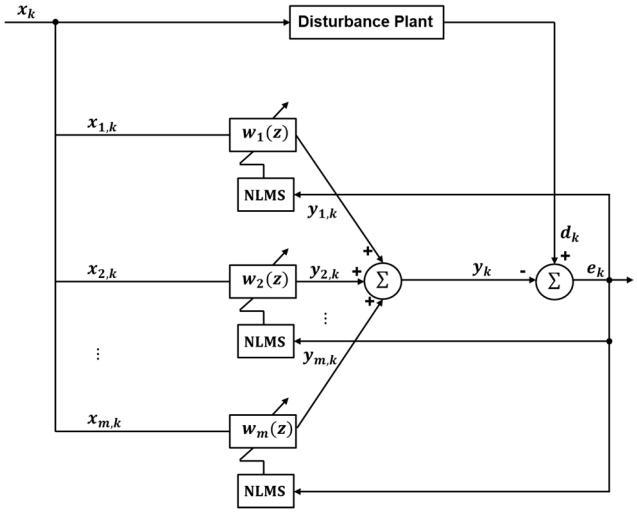

Fig. 6 Schematic for Multi-NLMS algorithm

modulated (AM) and frequency-modulated (FM) signals were used to confirm the vibration reduction effect when the multi-NLMS algorithm was applied. In Eq. (29), the AM signal consists of a sinusoid at 460 Hz, whose amplitude is modulated with a carrier signal at 160 Hz. Also, Eq. (30) shows the FM signal at 460 Hz, whose frequency is modulated with a carrier signal at 60 Hz.

3.2 Multi-NLMS algorithm

The adaptive filter can generate the desired signal for plants to perform control and analysis. These methods have an iterative algorithm, and using this characteristic, the filter coefficients are updated based on the error signal between the plant and filter output signal. Thus, these methods are widely used for active vibration and noise control. In this research, the sinusoid is controlled using the NLMS algorithm, and multi-frequency signals, such as AM and FM signals, are controlled based on multi-NLMS algorithm with three channels. A schematic of the multi-NLMS is shown in Fig. 6.

In Fig. 6, x_k and d_k represent the signals corresponding to the disturbance and the plant output, respectively. In addition, y_k represents the combined signal output from each filter, and e_k is the error signal between d_k and y_k. Furthermore, the weight update equation for the NLMS algorithm is expressed in Eq. (31).

$$w(k+1) = w(k) + \frac{\mu}{\alpha + X^T(k)X(k)} X(k)e(k) \quad (31)$$

To control the system through active mounting systems,

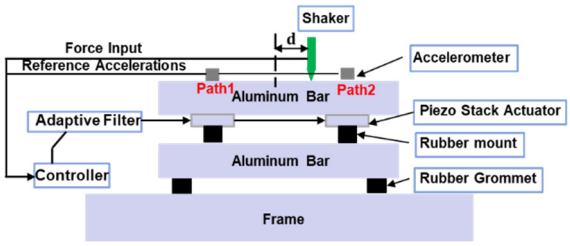

Fig. 7 Schematic of the structure with Multi-NLMS algorithm control

the location of the active mounting system in the source component is desired, and it is applied to the input signal for the active mounting system, as shown in Fig. 7.

3.3 Comparison of simulation results

A simulation was performed to compare the vibration reduction achieved by the quantification method and active vibration control. First, the quantification method results and the results of the active vibration control method, which is the NLMS algorithm, are summarized. To perform the simulation for the quantification method, the active mounting system input forces were calculated using Eq. (22), and the input signals are defined by Eqs. (32)-(33).

$$F_{ac1}(t) = F_1 \, sin(2\pi 460t + \phi_{st1}) \quad (32)$$

$$F_{ac2}(t) = F_2 \, sin(2\pi 460t + \phi_{st2}) \quad (33)$$

In Eqs. (32)-(33), F_1 and F_2 represent the amplitude, and these values are -10.0518 and -0.0254, respectively. In addition, ϕ_{st1} and ϕ_{st2} represent the phase, and the values are -6.0357 and 0.0431, respectively. The simulation was performed by applying the calculated values, and the results are shown in Fig. 8. The reduction rate of dB scale is summarized in Table 2.

In Table 2, the dB reduction rate of Path 1 was significantly decreased by 89.7 dB under the quantification method, whereas Path 2 decreased by 7.6 dB. To compare the performance of vibration reduction, the NLMS algorithm was applied to the active mounting system. As mentioned in Section 3.2, control was performed by tracking the source component signal at the location of the active mounting system. The simulation was performed using the NLMS algorithm, and the results are shown in Fig. 9. The reduction rate of dB scale is summarized in Table 3.

In Table 3, the dB reduction rate of Path 1 and Path 2 were significantly decreased by 54.6 and 49.2 dB, respectively. From these results, in the case of Path 1, the vibration reduction effect showed a greater performance under the quantification method than the NLMS algorithm. However, in the case of Path 2, a better performance was shown under the NLMS algorithm. Vibration control is required to decrease the overall vibration of the structure. However, for the quantification method, when calculating the force of the active mounting system, only one path was found to isolate the vibration. Thus, the vibration isolation effect was evident in Path 1 but did not contribute to

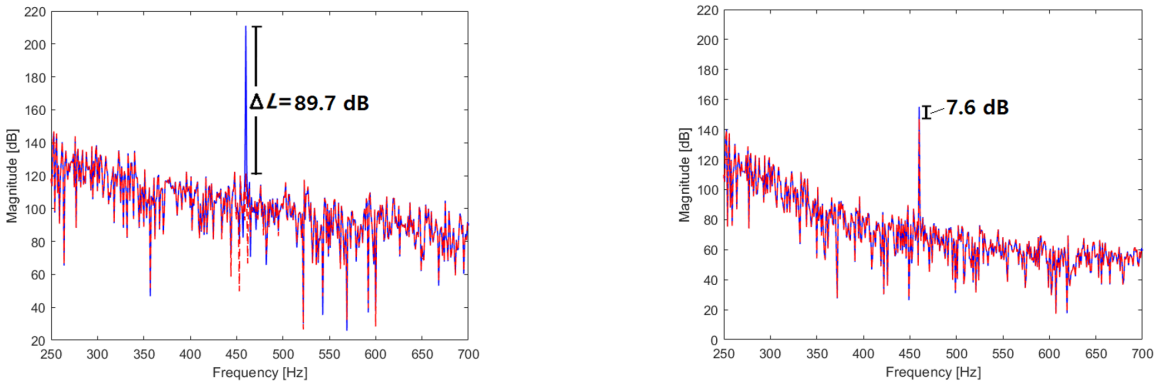

(a) Path 1 (b) Path 2

Fig. 8 Quantification method control on source part; key: ——— before control, - - - after control

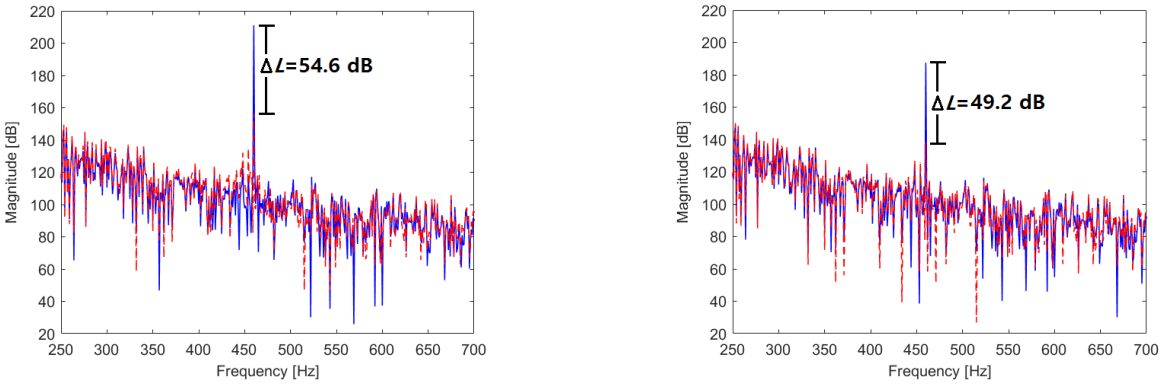

(a) Path 1 (b) Path 2

Fig. 9 NLMS algorithm control on source part; key: ——— before control, - - - after control

Table 2 Comparison of the peak values at 460 Hz in the frequency domain on source component-quantification method

Peak [dB]	Path 1	Path 2
Original	211.0	187.5
Quantification method	121.3	147.5
Decreasing rate	89.7 ↓	7.6 ↓

Table 3 Comparison of the peak values at 460 Hz in the frequency domain on source component-NLMS algorithm

Peak [dB]	Path 1	Path 2
Original	211.0	187.5
NLMS algorithm	156.4	138.3
Decreasing rate	54.6 ↓	49.2 ↓

vibration reduction in Path 2. Furthermore, the quantification method was difficult to apply to an actual engine system, because the engine generated a complex frequency. For the NLMS algorithm, both paths significantly decrease the vibration because when the inputs of each active mounting system were considered, each path signal was used as the system input through the NLMS algorithm. Additionally, the NLMS algorithm has been widely applied to actual control systems. Thus, the vibration reduction performance shows that the NLMS algorithm exerts a greater effect than the quantification method.

3.4 Simulation result for multi-frequency signals

An engine generates complex signals with many frequencies. Thus, to perform the appropriate active vibration control, multiple frequencies must be considered. Thus, multi-frequency signals, such as AM and FM signals, were applied to the structure to validate the vibration reduction performance for complex signals. First, the AM signal results are summarized and then the FM signal results are described. To validate the performance of the vibration reduction by applying the AM signal, a simulation was performed. The AM signal defined in Section 3.1 was applied, and the source signal was used as the control signal through the multi-NLMS, which was applied for appropriate adjustments. This study focused on the midfrequency range; therefore, the primary frequency of the AM signal was 460 Hz, and the sub-frequencies were 300 and 620 Hz. The simulation results are shown in Fig. 10. The reduction rate of dB scale is summarized in Table 4.

Path 1 results show that the primary frequency decreased by 27.9 dB, whereas the sub-frequencies

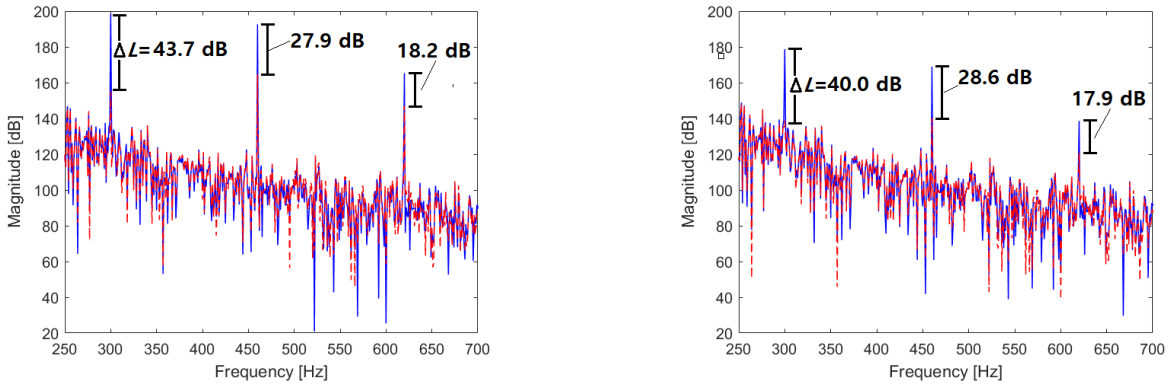

(a) Path 1 (b) Path 2

Fig. 10 AM signal on source part; key: original, multi-NLMS control

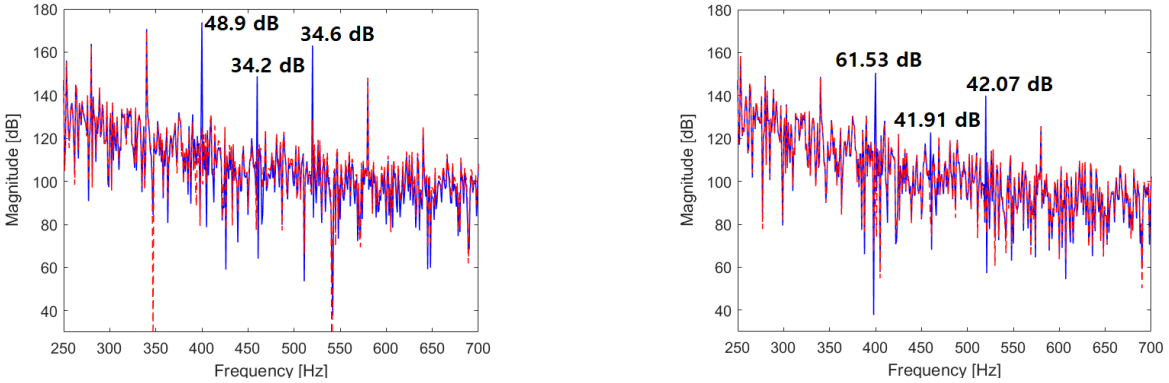

(a) Path 1 (b) Path 2

Fig. 11 FM Signal on Source part; key: original, multi-NLMS control

Table 4 Comparison of the peak values at the primary frequencies (300 Hz, 460 Hz, and 620 Hz) in the frequency domain

Peak [dB]		**Path 1**			**Path 2**	
Frequency	300 Hz	460 Hz	620 Hz	300 Hz	460 Hz	620 Hz
Original	198.6	192.6	165.3	178.7	168.9	138.6
NLMS Control	154.9	164.7	147.1	138.7	140.3	120.7
Decreasing Rate	43.7↓	27.9↓	18.2↓	40.0↓	28.6↓	17.9↓

Table 5 Comparison of the peak values at the primary frequencies (400 Hz, 460 Hz and 520 Hz) in the frequency domain

Peak [dB]		**Path 1**			**Path 2**	
Frequency	400 Hz	460 Hz	520 Hz	400 Hz	460 Hz	520 Hz
Original	173.8	148.7	163.0	150.5	122.8	139.9
NLMS Control	124.9	114.5	128.4	88.97	80.89	97.83
Decreasing Rate	48.9↓	34.2↓	34.6↓	61.53↓	41.91↓	42.07↓

decreased by 43.7 and 18.2 dB. Path 2 results show that the primary frequency decreased by 28.6 dB, whereas the sub-frequencies decreased by 40.0 and 17.9 dB. The simulation results show that the vibrations were significantly reduced when the multi-NLMS algorithm was applied in the active mounting systems. The AM signal was a simple signal with three frequencies; thus, to validate a more complex signal, the FM signal was used as a disturbance signal. The FM signal defined in Section 3.1 was applied. The FM signal exhibited a primary frequency of 460 Hz, and the carrier frequency was defined as 60 Hz. The source signal was used as the control signal through multi-NLMS, similarly as the AM signal. The simulation results are shown in Fig. 11. The reduction rate of dB scale is summarized in Table 5.

Path 1 results show that the primary frequency decreased by 34.2 dB, whereas the sub-frequencies decreased by 48.9 and 34.6 dB. Path 2 results show that the primary frequency decreased by 41.91 dB, whereas the sub-frequencies decreased by 61.53 dB and 42.07 dB. The simulation results of the AM and FM signals show that when multi-NLMS was applied in an active mounting system, the vibration reduction was significant. Furthermore, the source component could be controlled when an active mounting system consisting of a piezo actuator was used as a control path.

4. Conclusions

In this study, source motion control was performed using active mounting systems consisting of a piezoelectric actuator and rubber grommet when single- and multi-frequency signals were applied. The main contributions of this study are as follows: (1) To validate the control performance, a simulation was performed. The control performance confirmed that the NLMS performs better than the quantification method. (2) To confirm the vibration reduction performance of the complex signal, the AM and FM signals were used as excitation forces. Through simulations, the capability of control was demonstrated for complex signals.

To validate the control performance, the overall structure with the two active mounting systems was modeled based on a lumped parameter model. In addition, the active mounting system inputs were quantified through a mathematical method, which showed that the targeted path was isolated. However, this quantification method possesses several limitations. (1) It is applicable only to a single sinusoid. Thus, the quantification method could not be applied in real engine applications, owing to high signal complexity with multiple frequencies. (2) The trade-off was that the targeted path showed an isolation effect, whereas the other path is not affected. Thus, the NLMS algorithm was applied to the active mounting systems. To perform active control, the source component signal in the active mounting system was used as the input signal through appropriate adjustments. Vibration reduction was confirmed by comparing the quantification method and NLMS. The NLMS control effect showed a better performance than the quantification method. Practically, an actual engine generates complex signals with multiple frequencies. Thus, the multi-frequency capability was validated by applying AM and FM signals. In these cases, a multi-NLMS was applied, and the source component signal was used as the control signal. Through the simulation, when multi-NLMS was applied in an active mounting system, the vibration reduction was significant. Furthermore, the source component could be controlled when an active mounting system consisting of a piezo actuator was used as a control path. In future research, the structure should be expanded to consider the actual engine effect, because the current structure was modeled based on a simple beam. In addition, a feasibility experiment should be performed to confirm the simulation results. Also, further studies are required to optimize the number of target peaks (the number of channels for the multi-NLMS algorithm) for effective vibration reduction.

Acknowledgments

This work was supported by Basic Science Research Program through the National Research Foundation of Korea (NRF) funded by the Ministry of Education (NRF-2021R1A6A1A03039493 and NRF-2022R1F1A1076089).

References

ALamir, A.E. (2015), "Optimal control and design of composite laminated piezoelectric plates", *Smart Struct. Syst., Int. J.*, **15**(5), 1177-1202. https://doi.org/10.12989/sss.2015.15.5.1177

Cao, Y., Zandi, Y., Gholizadeh, M., Fu, L., Du, J., Qian, X., Wang, Z., Roco-Videla, A., Selmi, A. and Issakhov, A. (2021), "Optimization algorithms for composite beam as smart active control of structures using genetic algorithms", *Smart Struct. Syst., Int. J.*, **27**(6), 1041-1052. https://doi.org/10.12989/sss.2021.27.6.1041

Chee, C.Y., Tong, L. and Steven, G.P. (1999), "A mixed model for composite beams with piezoelectric actuators and sensors", *Smart Mater. Struct.*, **8**(3), 417-432. https://doi.org/10.1088/0964-1726/8/3/313

Choi, S.B. and Hong, S.R. (2007), "Active vibration control of a flexible structure using an inertial type piezoelectric mount", *Smart Mater. Struct.*, **16**, 25-35. https://doi.org/10.1088/0964-1726/16/1/003

Choi, S.B., Sohn, J.W., Han, Y.M. and Kim, J.W. (2008), "Dynamic characteristics of three-axis active mount featuring piezoelectric actuators", *J. Intell. Mater. Syst. Struct.*, **19**(9), 1053-1066. https://doi.org/10.1177/1045389X07083142

Gao, Z., Huang, J., Miao, Z. and Zhu, X. (2020), "Multiple model switching adaptive control for vibration control of cantilever beam with varying load using MFC actuators and sensors", *Smart Struct. Syst.., Int. J.*, **25**(5), 559-567. https://doi.org/10.12989/sss.2020.25.5.559

Garcia-Bonito, J., Brennan, M.J., Elliott, S.J., David, A. and Pinnington, R.J. (1998), "A novel high-displacement piezoelectric actuator for active vibration control", *Smart Mater. Struct.*, **7**, 31-42. https://doi.org/10.1088/0964-1726/7/1/005

Han, Y.M. (2020), "Experimental Investigation on Vibration Control Performances of the Piezoelectric Hybrid Mount", *J. Korea Converg. Soc.*, **11**(11), 203-209. https://doi.org/10.15207/JKCS.2020.11.11.203

Hillis, A.J., Harrison, A.J.L. and Stoten, D.P. (2005), "A comparison of two adaptive algorithms for the control of active engine mounts", *J. Sound Vib.*, **286**, 37-54. https://doi.org/10.1016/j.jsv.2004.09.023

Hong, D. and Kim, B. (2019a), "Vibration reduction against modulated excitation using multichannel NLMS algorithm for a structure with three active paths between plates", *J. Mech. Sci. Technol.*, **33**(10), 4673-4680. https://doi.org/10.1007/s12206-019-0910-0

Hong, D. and Kim, B. (2019b), "Quantification of Active Structural Path for Vibration Reduction Control of Plate Structure under Sinusoidal Excitation", *Appl. Sci.*, **9**(4), 711. https://doi.org/10.3390/app9040711

Jang, D.D., Park, J. and Jung, H.J. (2015), "Experimental investigation of an active mass damper system with time delay control algorithm", Smart Struct. Syst., Int. J., 15(3), 863-879. https://doi.org/10.12989/sss.2015.15.3.863

Jiang. J., Gao, W., Wang, L., Teng, Z. and Liu, Y. (2018), "Active vibration control based on modal controller considering structure-actuator interaction", *J. Mech. Sci. Technol.*, **32**(8), 3515-3521. https://doi.org/10.1007/s12206-018-0702-y

Kim, B., Washington, G.N. and Singh, R. (2012a), "Control of incommensurate sinusoids using enhanced adaptive filtering algorithm based on sliding mode approach", *J. Vib. Control*, **19**(8), 1265-1280. https://doi.org/10.1177/1077546312444659

Kim, B., Washington, G.N. and Singh, R. (2012b), "Control of modulated vibration using an enhanced adaptive filtering algorithm based on model-based approach", *J. Sound Vib.*, **331**(18), 4101-4114. https://doi.org/10.1016/j.jsv.2012.04.007

Kim, B., Washington, G.N. and Yoon, H.S. (2013), "Active vibration suppression of a 1D piezoelectric bimorph structure

using model predictive sliding mode control", *Smart Struct. Syst.*, *Int. J.*, **11**(6), 623-635. https://doi.org/10.12989/sss.2013.11.6.623

Lee, S.K., Lee, S., Back, J. and Shin, T. (2018), "A new method for active cancellation of engine order noise in a passenger car", *Appl. Sci.*, **8**(8), 1394. https://doi.org/10.3390/app8081394

Liette, J., Dreyer, J.T. and Singh, R. (2014), "Interaction between two active structural paths for source mass motion control over mid-frequency range", *J. Sound Vib.*, **333**(9), 2369-2385. https://doi.org/10.1016/j.jsv.2013.12.002

Lin, C.Y. and Jheng, H.W. (2017), "Active vibration suppression of a motor-driven piezoelectric smart structure using adaptive fuzzy sliding mode control and repetitive control", *Appl. Sci.*, **7**(3), 240. https://doi.org/10.3390/app7030240

Lu, L.Y., Lin, G.L., Chen, Y.S. and Hsiao, K.A. (2020), "Vertical equipment isolation using piezoelectric inertial-type isolation system", *Smart Struct. Syst.*, *Int. J.*, **26**(2), 195-211. https://doi.org/10.12989/sss.2020.26.2.195

Malgaca, L. and Karagulle, H. (2009), "Simulation and experimental analysis of active vibration control of smart beams under harmonic excitation", *Smart Struct. Syst.*, *Int. J.*, **5**(1), 55-68. https://doi.org/10.12989/sss.2009.5.1.055

Naseri, R., Talebi, H.A., Ohadi, A. and Fakhari, V. (2020), "A robust active control scheme for automotive engine vibration based on disturbance observer", *ISA Transactions*, **100**, 13-27. https://doi.org/10.1016/j.isatra.2019.11.005

Niu, W., Zou, C.Z., Li, B. and Wanga, W. (2019), "Adaptive vibration suppression of time-varying structures with enhanced FxLMS algorithm", *Mech. Syst. Signal Process.*, **118**, 93-107. https://doi.org/10.1016/j.ymssp.2018.08.009

Shin, Y.H., Kim, T.Y. and Lee, J.H. (2019), "Development of Hybrid Vibration Isolator by Inertial-Type Actuator and Wire Mesh Mount", *IEEE/ASME Transact. Mechatron.*, **24**(3), 1356-1367. https://doi.org/10.1109/TMECH.2019.2906656

Simonović, A.M., Jovanović, M.M., Lukić, N.S., Zorić, N.D., Stupar, S.N. and Ilić, S.S. (2016), "Experimental studies on active vibration control of smart plate using a modified PID controller with optimal orientation of piezoelectric actuator", *J. Vib. Control*, **22**(11), 2619-2631. https://doi.org/10.1177/1077546314549037

Sohn, J.W., Paeng, Y.S. and Choi, S.B. (2010), "An active mount using an electromagnetic actuator for vibration control: experimental investigation", *J. Mech. Eng. Sci.*, **224**(8), 1617-1625. https://doi.org/10.1243/09544062JMES1902

Song, P. and Zhao, H. (2018), "Filtered-x generalized mixed norm (FXGMN) algorithm for active noise control", *Mech. Syst. Signal Process.*, **107**, 93-104. https://doi.org/10.1016/j.ymssp.2018.01.035

Vijayakumar, M.P., Ashwin, U. and Raja, S. (2014), "Active vibration control of engine mount system of transport aircraft using PZT stack actuators", *J. Mechatron.*, **2**, 226-231. https://doi.org/10.1166/jom.2014.1057

Vivek, G., Manu, S. and Nagesh, T. (2011), "Mathematical modeling of actively controlled piezo smart structures: a review", *Smart Struct. Syst.*, *Int. J.*, **8**(3), 275-302. https://doi.org/10.12989/sss.2011.8.3.275

Xiong, S.L. and Shi, G. (2012), "Piezoelectric actuator design and application on active vibration control", *Proceedings of 2012 International Conference on Solid State Devices and Materials Science*, Macao, April.

Zhao, Y. and Wang, X. (2019), "A review of low-frequency active vibration control of seat suspension systems", *Appl. Sci.*, **9**(16), 3326. https://doi.org/10.3390/app9163326